

# High spin polarization and circular dichroism of topological surface states on $\text{Bi}_2\text{Te}_3$

M. R. Scholz,<sup>1</sup> J. Sánchez-Barriga<sup>1</sup>, D. Marchenko,<sup>1</sup> A.

Varykhalov,<sup>1</sup> A. Volykhov,<sup>2</sup> L. V. Yashina,<sup>2</sup> and O. Rader<sup>1</sup>

<sup>1</sup>*Helmholtz-Zentrum Berlin für Materialien und Energie,  
Elektronenspeicherring BESSY II, Albert-Einstein-Str. 15, D-12489 Berlin, Germany and*

<sup>2</sup>*Department of Chemistry, Moscow State University,  
Leninskie Gory, 1/3, 119992 Moscow, Russia*

## Abstract

Topological insulators have been successfully identified by spin-resolved photoemission but the spin polarization remained low ( $\sim 20\%$ ). We show for  $\text{Bi}_2\text{Te}_3$  that the in-gap surface state is much closer to full spin polarization with measured values reaching 80% at the Fermi level. When hybridizing with the bulk it remains highly spin polarized which may explain recent unusual quantum interference results on  $\text{Bi}_2\text{Se}_3$ . The topological surface state shows a large circular dichroism in the photoelectron angle distribution with an asymmetry of  $\sim 20\%$  the sign of which corresponds to that of the measured spin.

The topological insulator<sup>1-10</sup> was proposed in 2005 when its two-dimensional version, the quantum spin Hall insulator, was investigated taking the example of graphene<sup>1</sup>: Provided a sizeable spin-orbit interaction existed in that material, a corresponding electronic band gap opens at the otherwise gapless Dirac crossing point. If the sample geometry is chosen to be that of a one-dimensional graphene ribbon, then inside of the gap only the two-dimensional bulk states are forbidden but at the one-dimensional boundaries of the ribbon, edge states will cross this gap<sup>1</sup>. Due to time-reversal symmetry, these states form Kramers pairs of opposite spin and opposite propagation directions. These chiral Dirac fermion states are 100% spin polarized, and the carriers cannot backscatter without violating spin conservation<sup>11</sup>. Because the spin-orbit interaction was not large enough in graphene<sup>1</sup>, alternative systems were sought and identified in theory<sup>2</sup>. The quantum spin Hall phase was eventually realized in HgTe/Hg<sub>1-x</sub>Cd<sub>x</sub>Te quantum wells where one-dimensional and chiral edge states could be detected by their transport properties<sup>3</sup>.

Subsequently, three-dimensional topological insulators have been predicted where the spin-orbit gap is the gap of the three-dimensional bulk states and topological protection of the two-dimensional surface state is again guaranteed by time-reversal symmetry<sup>4-7</sup>. This prediction has particularly well been received in the surface science community because, on the one hand, angle-resolved photoelectron spectroscopy permits the direct measurement of two-dimensional surface states and, on the other hand, the concept shares important properties with the spin-orbit-driven Rashba effect which is currently under intense investigation in semiconductor heterostructures<sup>12</sup> as well as at metal surfaces<sup>13-15</sup> and quantum wells<sup>16</sup>. In fact, the chiral spin arrangement where the spin is tangential to the constant-energy surfaces is similar in the Rashba effect while the topological protection and single-spin character of the surface state are characteristic of the topological insulator [Fig. 1(a,b)].

A topological surface state is present if it crosses the Fermi energy ( $E_F$ ) an odd number of times between two time-reversal invariant points of the surface Brillouin zone<sup>4</sup>, and for a proper counting, spin resolution was shown to be indispensable<sup>8-10</sup>. Among the systems predicted to be topological insulators are Bi<sub>2</sub>Se<sub>3</sub> and Bi<sub>2</sub>Te<sub>3</sub><sup>4,17</sup> with trigonal crystal structure [Fig. 1(d)] and bandgaps large enough to enable applications in spin-dependent transport at room temperature. These materials are electronically simple with just one Dirac cone predicted<sup>4,17</sup> and measured at  $\bar{\Gamma}$ <sup>10,18,27</sup>. Spin-resolved photoemission confirms that the surface state of Bi<sub>2</sub>Te<sub>3</sub> is spin polarized and the spin polarization reverses indeed

between two-dimensional electron wave vectors  $+\mathbf{k}_{\parallel}$  and  $-\mathbf{k}_{\parallel}$ <sup>10</sup>.

When backscattering of carriers occurs at the surface, it involves a transition from  $+\mathbf{k}_{\parallel}$  to  $-\mathbf{k}_{\parallel}$  and thus would violate spin conservation if states at  $+\mathbf{k}_{\parallel}$  and  $-\mathbf{k}_{\parallel}$  are of opposite spin<sup>1</sup>. There is naturally high interest in proving and using this avoided backscattering in electron transport but this has met with difficulties<sup>19–23</sup>. On a local scale, scanning tunneling microscopy (STM) shows that electrons occupying the topological surface states are not backscattered by nonmagnetic surface impurities<sup>19</sup>. On the other hand, these electrons do backscatter from surface steps<sup>19,22</sup>. Recently, Landau levels of the topological surface state of  $\text{Bi}_2\text{Se}_3$  samples with a mobility of  $\sim 0.1 \text{ m}^2/(\text{Vs})$  were observed by STM but only upwards from the Dirac point<sup>25</sup>. On a macroscopic scale, undoped high mobility [ $> 2 \text{ m}^2/(\text{Vs})$ ]  $\text{Bi}_2\text{Se}_3$  samples showed a surface mobility less than the bulk one<sup>21</sup>.  $\text{Bi}_2\text{Se}_3$  thin film samples showed only bulk transport down to 50 nm thickness despite the simultaneous presence of the Dirac cone in photoemission<sup>23</sup>. Doping of  $\text{Bi}_2\text{Se}_3$  by Ca can overcome its  $n$ -type self-doping and move  $E_{\text{F}}$  into the bulk gap<sup>20</sup>. In quantum interference experiments, a spin-based magnetofingerprint, i. e., conductance versus magnetic field, was measured which was found inconsistent with surface states but consistent with bulk states provided that those share a similar spin arrangement with the topological surface state<sup>20</sup>. On compositionally modulated bulk-insulating  $\text{Bi}_2\text{Te}_3$  samples, Shubnikov-de Haas oscillations have most recently been measured giving surface mobilities of  $\sim 1.0 \text{ m}^2/(\text{Vs})$ <sup>26</sup>.

At the present stage, several questions remain open. The spin polarization of the topological surface states of  $\text{Bi}_2\text{Te}_3$  has been measured by photoemission at  $E_{\text{F}}$ <sup>10</sup>. It shows a peak and reverses between  $+\mathbf{k}_{\parallel}$  and  $-\mathbf{k}_{\parallel}$ , as expected, but the spin polarization reaches only  $\sim 20\%$  which is unlikely caused by overlapping  $+$  and  $-100\%$  polarized peaks as has been suggested<sup>10</sup>. We investigate at first whether the spin polarization is intrinsically limited or whether it is only subject to extrinsic effects that can be technically overcome.

Single crystals of  $\text{Bi}_2\text{Te}_3$  and  $\text{Bi}_2\text{Se}_3$  were grown from melt by the Bridgman method. The entire 10 cm long crystals could be cleaved along their length, indicating the high quality and absence of twinning deformations. The growth time including cooling was about 2 weeks for a 40–50 g crystal. Using an adhesive tape, surfaces have been prepared in ultrahigh vacuum by *in situ* cleavage along the trigonal axis which produced (00·1) surfaces in hexagonal coordinates [(111) in rhombohedral coordinates].  $E(\mathbf{k}_{\parallel})$  dispersion relations and constant energy surfaces have been measured with a Scienta SES100 electron energy analyzer at the

UE112-PGM2a beamline of BESSY II with  $s$ ,  $p$ ,  $\sigma+$ , and  $\sigma-$  polarized undulator radiation. The incidence angle  $\beta$  was  $45^\circ$ . At the PGM1 branch, spin- and angle-resolved photoemission has been measured with linearly polarized light. The spin-resolved experiment measures the spin component in the surface plane of the sample and perpendicular to  $\mathbf{k}_{\parallel}$  and averages over a sample area of the order of  $500\mu\text{m} \times 500\mu\text{m}$  and over a  $\mathbf{k}_{\parallel}$  range of  $\pm 0.025 \text{ \AA}^{-1}$ . We found that cutting the samples perpendicular to the cleavage plane should be done without applying pressure so that the damage is limited to the periphery of the sample. This can be seen by changes in the low-energy electron diffraction (LEED) and a position dependence in angle-resolved photoemission. Control of this together with the successful in situ cleavage was found to be the main factor in obtaining high spin polarization, and we believe that our lower values for  $\text{Bi}_2\text{Se}_3$  are also due to imperfect samples.

Figure 1c indicates with an arrow the van-der-Waals-type (00·1) cleavage plane, which we characterized by LEED at 80 eV [Fig. 1(e)]. Figure 1e shows a characterization of  $\text{Bi}_2\text{Te}_3$  by angle-resolved photoemission where Fig. 1(f) (top) shows the topological surface state (TSS), the Dirac point ( $E_D$ ), and the valence band maximum (VBM). Different from the simple topological insulator model<sup>1</sup>, the Dirac point in  $\text{Bi}_2\text{Te}_3$  lies in the valence band which in principle would enable the topological surface state to couple to bulk states. The position of the conduction band minimum (CBM) (which does not appear here due to the  $\mathbf{k}_{\perp}$  respectively photon-energy dependence of the photoemission transition) indicates that the probed sample region is  $n$ -doped in agreement with our Hall-effect measurements. Along  $\bar{\Gamma}-\bar{M}$ , the linear dispersion of the surface state changes within 100 meV of  $E_F$  to a dispersion with smaller group velocity. This is related to the warping of the constant energy surface away from the circular shape at 100 meV binding energy seen in Fig. 1(g). It confirms previous measurements for  $(\text{Bi}0.67\%\text{Sn})_2\text{Te}_3$  and  $\text{Bi}_2\text{Te}_3$ <sup>27</sup> and investigations in theory<sup>28</sup>. The warping is predicted to lift the prohibition of backscattering<sup>28</sup>. Within 100 meV from  $E_D$ , the constant energy surface is, however, isotropic. The data in Fig. 1(f) (bottom) was measured under the same conditions as in Fig. 1(f) (top) but with s-polarized light which confirms the even symmetry of the topological surface state and of the bulk state below  $E_D$ .

Figure 2a shows spin- and angle-resolved photoemission data for  $\text{Bi}_2\text{Te}_3$  at 50 eV photon energy. The data was measured at  $\mathbf{k}_{\parallel} = 0.11 \text{ \AA}^{-1}$  and for  $\text{Bi}_2\text{Se}_3$  in Fig. 2b at  $0.09 \text{ \AA}^{-1}$  approximately following  $\bar{\Gamma}-\bar{K}$ . We show the photoemission intensity for spin up ( $I^{\uparrow}$ ) and spin down ( $I^{\downarrow}$ ) along with the detected spin asymmetry  $[(I^{\uparrow} - I^{\downarrow})/(I^{\uparrow} + I^{\downarrow})]$ . The spin-resolved

count rate from  $\text{Bi}_2\text{Te}_3$  and  $\text{Bi}_2\text{Se}_3$  is rather low even as compared to the background counts so that the spin asymmetry is reduced accordingly. Therefore, we determine above  $E_F$  the background intensity  $I_B$  (horizontal line in Fig. 2) and plot the intrinsic spin polarization  $[(I^\uparrow - I^\downarrow)/(I^\uparrow + I^\downarrow - 2I_B)]$ . (Note that some extremely large error bars in the spin polarization result merely from formally negative intensities after the background subtraction.) We see that the topological surface state of  $\text{Bi}_2\text{Te}_3$  is close to 100% spin polarized  $[(82 \pm 10)\%$  spin polarization for binding energies 0.02 to 0.18 eV]. Many cleavages, however, resulted in lower spin polarization around 50%, and for  $\text{Bi}_2\text{Se}_3$  we did not obtain cleavages yielding more than 25% for the topological surface state, most likely due to sample imperfections. (Note that the sign of the spin polarization in Fig. 2b is reversed because also the emission angle is reversed with respect to Fig. 2a.) The fact that a spin polarization not too far from 100% can be measured means that this quantity is not principally limited to values around 20% measured previously, and it confirms the previous interpretation as topological surface state<sup>10</sup>.

In Fig. 2 we have marked besides the TSS also the bulk state (BS) which is connected to it through the Dirac point [see Fig. 1(f)]. For  $\text{Bi}_2\text{Te}_3$ , the band structure calculation<sup>18</sup> assigns BS unambiguously to bulk. For  $\text{Bi}_2\text{Se}_3$ , BS means rather bulk and/or surface because the calculation<sup>18</sup> shows a perfect lower half of the Dirac cone of the topological surface state while in experiment it is filled with bulk states<sup>17</sup>. For both systems the states BS (as well as BS<sub>2</sub>) are highly spin polarized with a polarization of  $-22\%$  for  $\text{Bi}_2\text{Te}_3$  ( $36\%$  for BS of  $\text{Bi}_2\text{Se}_3$  in Fig. 2b) and a reversal of the spin at  $E_D$  as expected for the topological insulator. TSS and BS can and must hybridize as they share the same symmetry [see Fig. 1(f)]. As a bulk state is principally unpolarized due to bulk inversion symmetry within the quintuple layer [Fig. 1(d)], this means for  $\text{Bi}_2\text{Te}_3$  that bulk states are below  $E_D$  hybridized with the topological surface state and in this way can acquire a spin polarization<sup>32</sup>. For  $\text{Bi}_2\text{Se}_3$  possibly the same happens. Therefore, the postulation of a strong hybridization of topological surface states with bulk states under transfer of the locking of spin and momentum direction to explain the magnetic fingerprint data of  $\text{Bi}_2\text{Se}_3$  is not unrealistic<sup>20</sup> but at least transport below  $E_D$  must be characterized by degenerate TSS and bulk states. Note that an unusual coupling of topological surface states with bulk states was also reported for  $\text{Bi}_{10}\text{Sb}$ <sup>24</sup>.

We also applied circular dichroism in the angle distribution (CDAD) of photoelectrons to  $\text{Bi}_2\text{Te}_3$ . In this case, a spin polarimeter is not required and, instead, photoemission spectra

are recorded subsequently for  $\sigma+$  and  $\sigma-$  light. It is important to note that the circular dichroism does not directly couple to the electron spin. This distinguishes this method from spin-resolved photoemission. In an atomic description, the spin effect enters via the spin-orbit coupling since the light interacts with the orbital angular momentum. Generally, a circular dichroism effect occurs if the system and the photoemission geometry [Fig. 1(c)] with  $\sigma+$  and  $\sigma-$  light are inequivalent. In the present case, the symmetry of the system is lowered by the spin-orbit interaction. The valence-band photoemission is described by a matrix element with initial- and final-state wave functions. The matrix element depends on how the double-group representation of the dipole operator which includes the direction of circular polarization relates to those of the initial and final state which include the spin. In ferromagnetic transition metals, spin-dependent circular dichroism effects of up to 5% dichroism asymmetry  $[(I_{\sigma+} - I_{\sigma-})/(I_{\sigma+} + I_{\sigma-})]$  have been measured<sup>29-31</sup>.

Figure 3a shows that for  $\sigma+$  light TSS is more intense for positive than for negative emission angles, while for  $\sigma-$  light it is the opposite. The dichroism effect amounts to 20% (e. g., at 0.1 eV binding energy). When we follow the TSS through the Dirac point into BS, we see that the dichroism asymmetry reverses exactly as the spin does in Fig. 1 and 2. This is an indication that the present measurement may probe the angular momentum to which the spin is coupled through strong spin-orbit coupling. Note that in  $\text{Bi}_2\text{Te}_3$ , the spin-orbit interaction is much larger than for the ferromagnetic transition metals due to higher atomic numbers.

As in the present work we combine the methods of spin- and angle-resolved photoemission and of circular dichroism in the angle dependence of photoemission, we can confirm that the observed large circular dichroism of the topological surface state and the connected bulk state BS does correspond to a large spin polarization and its wave-vector dependence. We cannot, at present, prove that the spin *via* the angular momentum is the reason of the strong circular dichroism. Also band-like states of light elements ( $Z = 6$ ) have shown large circular dichroism effects in the angle distribution<sup>33</sup>. In this situation, only a photoemission calculation taking into account the photoemission final state can clarify the origin of the strong circular dichroism effect of the topological surface state.

In conclusion, we observe that the spin polarization measured from the in-gap surface state of  $\text{Bi}_2\text{Te}_3$  and  $\text{Bi}_2\text{Se}_3$  requires careful cleaving but that high values not too far from 100% can be obtained with methods which integrate over macroscopic areas of  $\sim 0.25 \text{ mm}^2$ .

The degeneracy of surface and bulk states below the Dirac point leads, at least for  $\text{Bi}_2\text{Te}_3$ , via hybridization to a bulk state which has the spin topology of the topological surface state imposed. A large circular dichroism effect in the angle distribution of photoelectrons is measured which, with the help of the spin-resolved data, is shown to point along the spin of the electrons. The circular dichroism does not require special detectors and allows for count rates which are by 2 to 3 orders of magnitude larger than with spin-resolved photoemission. It is, therefore, worthwhile investigating by a photoemission calculation whether or not the present dichroism measures *via* the angular momentum indirectly the spin structure.

- 
- <sup>1</sup> C. L. Kane and E. J. Mele, Phys. Rev. Lett. 95, 146802 (2005); Phys. Rev. Lett. 95, 226801 (2005).
- <sup>2</sup> B. A. Bernevig and S. C. Zhang, Phys. Rev. Lett. 96 106802 (2006).
- <sup>3</sup> M. König *et al.*, Science 318, 766 (2007).
- <sup>4</sup> Liang Fu, C. L. Kane, and E. J. Mele, Phys. Rev. Lett. 98, 106803 (2007).
- <sup>5</sup> J. E. Moore and L. Balents, Phys. Rev. B 75, 121306 (2007).
- <sup>6</sup> R. Roy, Phys. Rev. B 79, 195322 (2009).
- <sup>7</sup> S. Murakami, New J. Phys. 9, 356 (2007).
- <sup>8</sup> D. Hsieh *et al.*, Science 323, 920 (2009).
- <sup>9</sup> J. W. Wells *et al.*, Phys. Rev. Lett. 102, 096802 (2009).
- <sup>10</sup> D. Hsieh *et al.*, Nature 460, 1101 (2009).
- <sup>11</sup> Already the two-dimensional bulk states in graphene have without spin-orbit coupling a similar property due to the conservation of the valley or isospin: T. Ando, T. Nakanishi, and R. Saito, J. Phys. Soc. Jpn. 67, 2857 (1998); M. Katsnelson, K. S. Novoselov, and A. K. Geim, Nature Phys. 2, 620 (2006).
- <sup>12</sup> J. Nitta, T. Akazaki, H. Takayanagi, and T. Enoki, Phys. Rev. Lett. 78, 1335 (1997).
- <sup>13</sup> S. LaShell, B. A. McDougall, and E. Jensen, Phys. Rev. Lett. 77, 3419 (1996); F. Reinert *et al.*, Phys. Rev. B 63, 115415 (2001); M. Hoesch *et al.*, Phys. Rev. B 69, 241401(R) (2004).
- <sup>14</sup> T. Hirahara *et al.*, Phys. Rev. B 76, 153305 (2007).
- <sup>15</sup> C. R. Ast *et al.*, Phys. Rev. B 75, 201401(R) (2007).

- <sup>16</sup> A. Varykhalov *et al.*, Phys. Rev. Lett. 101, 256601 (2008); J. H. Dil *et al.*, Phys. Rev. Lett. 101, 266802 (2008); J. H. Dil, J. Phys.: Condens. Matter 21, 403001 (2009).
- <sup>17</sup> H. Zhang *et al.*, Nature Phys. 5, 438 (2009).
- <sup>18</sup> Y. Xia *et al.*, Nature Phys. 5, 398 (2009).
- <sup>19</sup> T. Zhang *et al.*, Phys. Rev. Lett. 103, 266803 (2009).
- <sup>20</sup> J. G. Checkelsky *et al.* Phys. Rev. Lett. 103, 246601 (2009).
- <sup>21</sup> N. P. Butch *et al.*, arXiv: 1003.2382v1 (2010).
- <sup>22</sup> P. Roushan *et al.*, Nature 460, 1106 (2009).
- <sup>23</sup> J. G. Analytis *et al.*, Phys. Rev. B 81, 205407 (2010).
- <sup>24</sup> A. A. Taskin and Y. Ando, Phys. Rev. B 80, 085303 (2009).
- <sup>25</sup> P. Cheng *et al.*, Phys. Rev. Lett. 105, 076801 (2010).
- <sup>26</sup> D.-X. Qu *et al.*, Science 329, 821 (2010).
- <sup>27</sup> Y. L Chen *et al.*, Science 325, 178 (2009).
- <sup>28</sup> Liang Fu, Phys. Rev. Lett. 103, 266801 (2009).
- <sup>29</sup> J. Bansmann *et al.*, Surf. Sci. 269/270, 622 (1992).
- <sup>30</sup> W. Kuch and C. M. Schneider, Rep. Prog. Phys. 64, 147 (2001).
- <sup>31</sup> We do not discuss here circular dichroism of localized states such as core levels or semi-core  $4f$  orbitals which do not show a dispersion with  $\mathbf{k}$  and for which angular moments are well defined and selection rules are straightforward.
- <sup>32</sup> An alternative explanation for polarization of bulk-like states in the outermost atomic layers was given recently for Bi metal by A. Kimura *et al.*, Phys. Rev. Lett. 105, 076804 (2010).
- <sup>33</sup> G. Schönhense, C. Westphal, J. Bansmann, and M. Getzlaff, Europhys. Lett. 17, 727 (1992).



## Figure captions

Figure 1. (Color online) Band topology of a spin-orbit split surface state for (a) the Rashba effect and (b) the topological insulator for the example of  $\text{Bi}_2\text{Te}_3$ . (c) Photoemission geometry. (d) Structure and cleavage plane (not to scale). (e) Brillouin zone and LEED pattern at 80 eV. (f) Angle-resolved photoemission at 50 eV photon energy along  $\bar{\Gamma}\text{-}\bar{M}$ . The topological surface state (TSS) appears in the band gap between the valence-band maximum (VBS) and the conduction-band minimum (CBM, taken from 30 eV data) and the two become degenerate at the Dirac point ( $E_D$ ).  $p$ - and  $s$ -polarized light reveal symmetry properties. (g) Constant energy surfaces of the topological surface state including the Fermi surface from photoemission at 50 eV photon energy.

Figure 2. (Color online) Spin- and angle-resolved photoemission of the topological surface state for  $\text{Bi}_2\text{Te}_3$  and  $\text{Bi}_2\text{Se}_3$ . Spin up ( $\triangle$ ), spin down ( $\nabla$ ), spin asymmetry (from raw data), and spin polarization spectrum (background subtracted) ( $\diamond$ ). Note that the spectra in (a) and (b) were taken on opposite sides of normal emission ( $\bar{\Gamma}$ ). The bulk band gap is marked. The magnitude of the spin polarization of the topological surface state feature amounts to  $(82 \pm 10)\%$  for  $\text{Bi}_2\text{Te}_3$  and  $(24 \pm 15)\%$  for  $\text{Bi}_2\text{Se}_3$ . BS, which is predicted to be bulk for  $\text{Bi}_2\text{Te}_3$ , is highly spin polarized as well.

Figure 3. (Color online) Circular dichroism of the topological surface state of  $\text{Bi}_2\text{Te}_3$ . (a) Angle-resolved photoemission intensity  $I$  for  $\sigma+$  light and  $\sigma-$  light along with the dichroism  $[I(\sigma+) - I(\sigma-)]/[I(\sigma+) + I(\sigma-)]$ . (b) Constant-energy cuts at various binding energies  $E_B$ . For the topological surface state we see above  $E_D$  a circular dichroism effect of 20% (at 0.1 eV binding energy). (c) Dichroism spectra measured for a similar  $\mathbf{k}_{\parallel}$  at  $E_F$  [see dashed lines in (a)] as in Fig. 2. The photon energy is 50 eV.

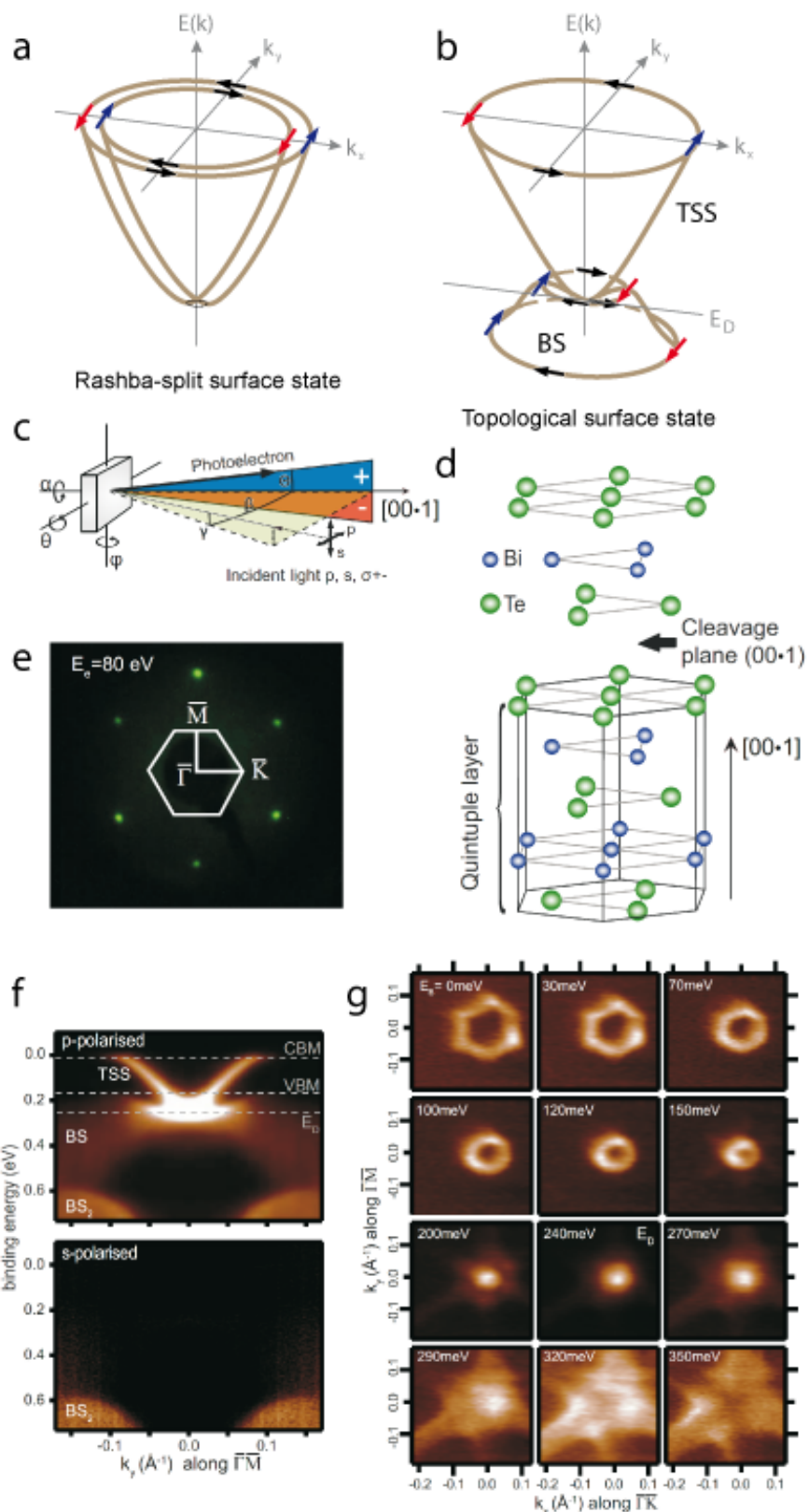


Figure 1

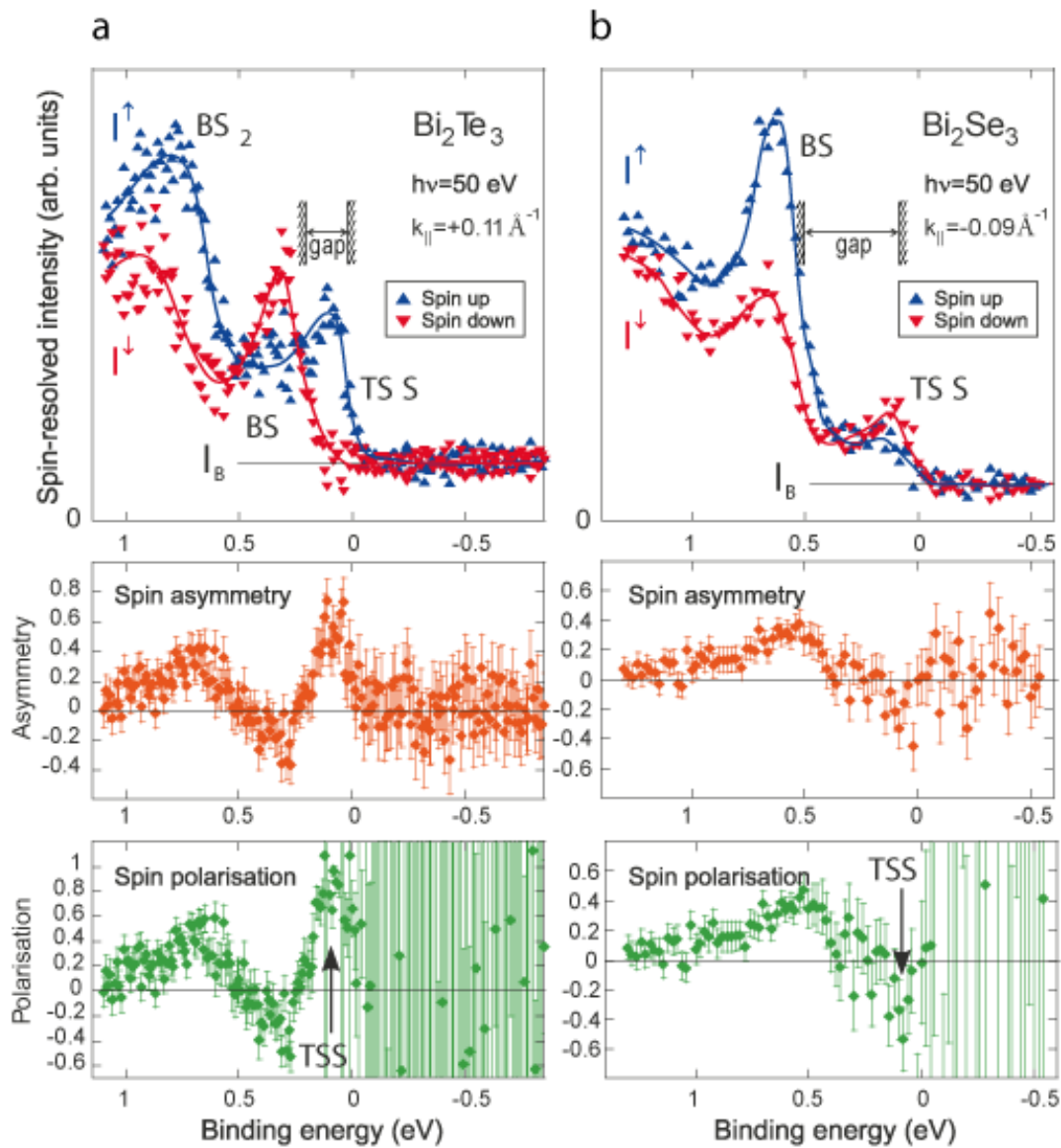


Figure 2

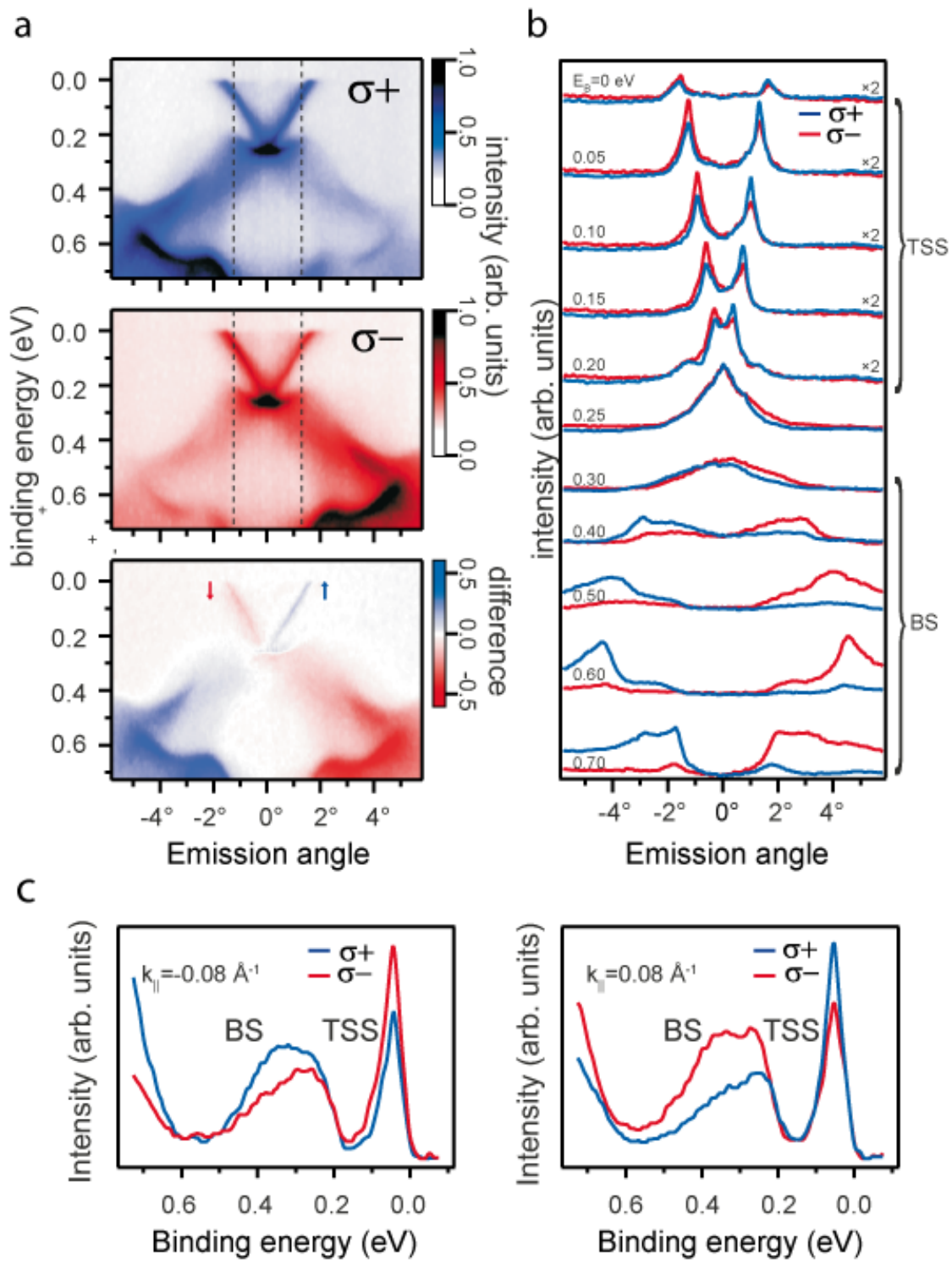


Figure 3